Title	Three-dimensional graphene foam supported Fe3O4 lithium battery anodes with long cycle life and high rate capability
Author(s)	Luo, Jingshan; Liu, Jilei; Zeng, Zhiyuan; Ng, Chin Fan; Ma, Lingjie; Zhang, Hua; Lin, Jianyi; Shen, Zexiang; Fan, Hong Jin
Citation	Luo, J., Liu, J., Zeng, Z., Ng, C. F., Ma, L., Zhang, H., Lin, J., Shen, Z., & Fan, H. J. (2013). Three-Dimensional Graphene Foam Supported Fe3O4 Lithium Battery Anodes with Long Cycle Life and High Rate Capability. Nano Letters, 13 (12), 6136–6143.
Date	2013
URL	http://hdl.handle.net/10220/17791
Rights	© 2013 American Chemical Society. This is the author created version of a work that has been peer reviewed and accepted for publication by Nano Letters, American Chemical Society.. It incorporates referee's comments but changes resulting from the publishing process, such as copyediting, structural formatting, may not be reflected in this document. The published version is available at: [http://dx.doi.org/10.1021/nl403461n].

Communication

3D Graphene Foam Supported Fe3O4 Lithium Battery Anodes with Long Cycle Life and High Rate Capability

Jingshan Luo, Jilei Liu, Zhiyuan Zeng, Chin Fan Ng, Lingjie Ma, Hua Zhang, Jianyi Lin, Zexiang Shen, and Hong Jin Fan

Nano Lett., **Just Accepted Manuscript** • Publication Date (Web): 12 Nov 2013

3D Graphene Foam Supported Fe_3O_4 Lithium Battery Anodes with Long Cycle Life and High Rate Capability

Jingshan Luo,[†] Jilei Liu,[†] Zhiyuan Zeng,[‡] Chi Fan Ng,[†] Lingjie Ma,[†] Hua Zhang,[‡] Jianyi Lin,[†,#] Zexiang Shen, [†,‡, §] Hong Jin Fan[†,§,*]

[†]*Division of Physics and Applied Physics, School of Physical and Mathematical Sciences, Nanyang Technological University, 637371, Singapore*
[‡]*School of Materials Science and Engineering, Nanyang Technological University, 639798, Singapore*
[§]*Centre for Disruptive Photonic Technologies, Nanyang Technological University, 637371, Singapore*
[#] *Heterogeneous Catalysis, Institute of Chemical Engineering and Sciences, A*star, 1 Pesek Road, Jurong Island, 627833, Singapore*

ABSTRACT

Fe_3O_4 has long been regarded as a promising anode material for lithium ion battery due to its high theoretical capacity, earth abundance, low cost and nontoxic properties. However, up to now, no effective and scalable method has been realized to overcome the bottleneck of poor cyclability and low rate capability. In this article, we report a bottom up strategy assisted by atomic layer deposition (ALD) to graft bicontinuous mesoporous nanostructure Fe_3O_4 onto three dimensional (3D) graphene foams and directly use the composite as the lithium ion battery anode. This electrode exhibits high reversible capacity and fast charging and discharging capability. A high capacity of 785 mAh/g is achieved at 1C rate and is maintained without decay up to 500 cycles. Moreover, the rate of up to 60C is also demonstrated, rendering a fast discharge potential. To our knowledge, this is the best reported rate performance for Fe_3O_4 in lithium ion battery to date.

KEYWORDS: 3D Graphene foam · Iron oxide · Lithium ion battery · Atomic layer deposition · High rate capability · Li ion storage

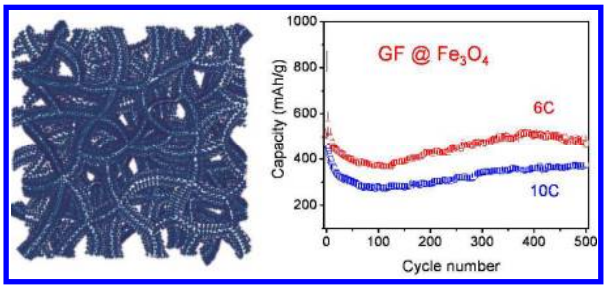

TOC Figure

The emergence of electric vehicles and power grid applications demands lithium ion batteries (LIB) with both high energy capacity and power density.[1, 2] This requires a scrupulous selection of materials and design of nanostructures which allow fast charge-discharge rate capability. Fe_3O_4 with a high theoretical energy capacity (around three times of graphite), earth abundance and low cost has long been considered as a promising anode material.[3, 4] However, the large volume expansion and the low conductivity characteristics of Fe_3O_4 hinder its stable performance.[4] A breaking down of electrical connection of Fe_3O_4 from current collectors due to high volume changes during continuous charge–discharge process has been reported, which significantly limits its practical application.[5] During the past decades, tremendous efforts have been made to overcome these issues, which can be generally summarized into two categories: one is building nanostructures;[3, 6-8] the other is combining Fe_3O_4 with conductive substrates [4, 9-13]or other stable metal oxides.[14, 15]

Building nanostructures is a primary and popular strategy to improve the performance of the LIB electrode, as nanostructures have several advantages over their bulk counterparts.[3, 13, 16-18] First, a nanostructure has a short transport path which could shorten the Li ions diffusion time. Second, the nanostructure has an increased electrode/electrolyte contact area that is beneficial to the high current rate performance. More importantly, with nanostructures, the strain could be significantly reduced during lithiation and dilithiation process, thus preserving the structural integrity of the electrode and leading to a more stable cycle performance. Motivated by these advantages, various nanostructures have been designed to enhance the performance of iron oxide LIB electrodes, such as nanoparticles,[19] nanowires,[20] nanotubes,[6] nanowalls,[21] porous nanosheets[22] and hollow nanoparticles.[23] To further increase the conductivity and reduce the diffusion length, Fe_3O_4 has been combined with various metal nanostructures,[4] polymers,[24] carbon materials[10, 11, 13] and other stable materials.[15] The development of carbon materials, from amorphous carbon, carbon nanotubes to more recently graphene leads to the hybridization of Fe_3O_4 with carbon materials into a new path towards success. In particular, graphene,[9, 22, 25] which has an excellent electrical conductivity, high mechanical flexibility, large specific surface area and pronounced thermal and chemical stability,[26] provides great opportunity in improving the performance of Fe_3O_4 as the LIB electrodes.

Despite the progress mentioned above, the performance enhancement of Fe_3O_4 LIB electrode is still marginal. To our knowledge, so far there is no report on Fe_3O_4 based electrodes that can

demonstrate long cycle life up to hundreds of cycles with a fast charge discharge capability. In this article, we demonstrate a new while relatively simple bottom up strategy to build bicontinuous[18] mesoporous Fe_3O_4 nanostructures grafted onto the graphene foam. Such a unique LIB electrode structure has following characteristics: *First*, the 3D graphene foam grown by chemical vapor deposition (CVD) has a high electrical conductivity (around 1000 S/m) that ensures an efficient ion and electron transportation.[26, 27] In addition, the 3D graphene foam is extremely light and flexible compared to other 3D bulk metal electrodes such as Ni foams. This is highly desirable for developing the power source for portable and flexible electronics. *Second*, the bicontinuous Fe_3O_4 nanostructure is formed by interconnected nanocrystallites which are homogenously distributed on the graphene foam surface with a close physical contact. The direct contact and interconnection provide an efficient lithium ion and electron transport between Fe_3O_4 and graphene, as well as ion transport between the electrolyte and the active material.[18] With this design, the graphene foam can be directly employed as the current collector without binder and conducting agent, so that the intact contact between Fe_3O_4 and graphene foam can prevent not only the aggregation of Fe_3O_4 particles, but also the breaking-down of electric connection between the active material and the current collector due to the volume change during long cycles of charge and discharge. *Finally*, as the Fe_3O_4 is obtained from a uniform-thickness ZnO sacrificial layer, the loading of Fe_3O_4 can thus be tuned by varying the ZnO layer thickness. This allows a high amount of active material within the electrode. In a nutshell, the as-fabricated 3D architectures may satisfy nearly all kinetic requirements for long cycle life and fast charging and discharging of an ideal electrode material. We demonstrate the charge and discharge of the hybrid electrode up to 500 cycles with the capacity of ~780 mAh/g at 1C and ~350 mAh/g at 10C.

Fabrication of GF@Fe_3O_4 composite. Graphene foam rather than the other carbon materials was chosen because of its excellent conductivity, 3D porous structure, flexible and freestanding property. The bicontinuous mesoporous Fe_3O_4 nanostructure was deposited on the graphene surface by the ZnO sacrificial layer assisted hydrolysis.[28] The fabrication process of the graphene foam supported Fe_3O_4 nanostructure electrodes (GF@Fe_3O_4) is composed of three steps (see schematics in Figure 1). For the 1st step, graphene foam was grown on Ni foam by CVD and then Ni was etched away by a mixture of $FeCl_3$ and HCl solution following the previous reports (Fig. 1a).[27] In the 2nd step, a layer of ZnO was coated onto the graphene foam by atomic layer

deposition (ALD) (Fig. 1b). ALD is a thin film deposition technique that is based on self-limiting surface reactions by sequential exposure of the substrate to different gas phase precursors, which could provide precise thickness control and homogenous coating of active materials on various substrates.[29, 30] Previously we have applied ALD for the fabrication of 3D inverse opal photoelectrochemical electrodes.[29, 31] As the basal plane of graphene is chemically inert, to ensure conformal and homogeneous coating of ZnO, the graphene foams were treated by oxygen plasma before ALD to create the hydroxyl bonds on the surface.[32, 33] In the last step, the ZnO coated graphene foams were bathed into the $FeCl_3$ solution mixed with glucose. After annealing at 400°C in an Ar atmosphere, the bicontinuous mesoporous Fe_3O_4 nanostructure on graphene foam was obtained (Fig. 1c). The glucose here was used to form a layer of amorphous carbon on the Fe_3O_4 surface after high temperature pyrolysis.[13] This indirect ALD ZnO sacrificial layer assisted deposition of Fe_3O_4 on graphene foam could circumvent the challenges of direct ALD Fe_2O_3 on graphene, which has a very low growth rate and thus low iron oxides loading, and needs high temperature and ozone atmosphere.[34, 35] More pronouncedly, this method can form the unique bicontinuous mesoporous nanostrucure rather than a compact thin film.

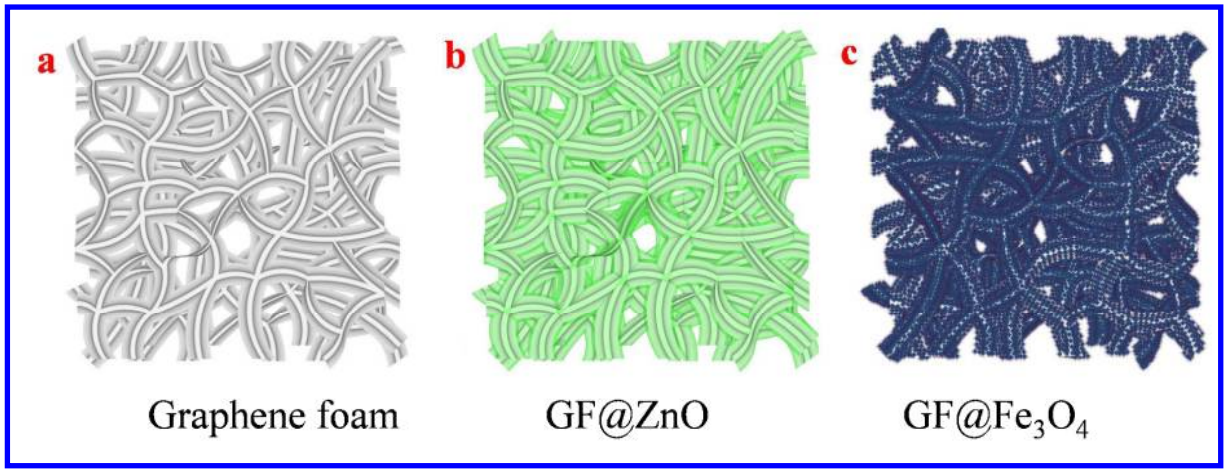

Figure 1. Schematic diagram of the sample structure. (a) graphene foam backbone. (b) graphene foam coated with ZnO by atomic layer deposition (GF@ZnO). (c) graphene foam supported Fe_3O_4 nanostructure electrodes (GF@Fe_3O_4).

Structural characterization. To reveal the structure and composition of the electrodes in each step, X-ray diffraction (XRD), Raman spectroscopy and XPS analysis were carried out. Results

are shown in Fig. 2. The as grown graphene foam shows two typical diffraction peaks at 26.5° and 54.6°, attributed to the (002) and (004) reflections of graphitic carbon, respectively (JCPDS card 75-1621).[36] The high crystalline structure of graphene is favorable for the ion diffusion and

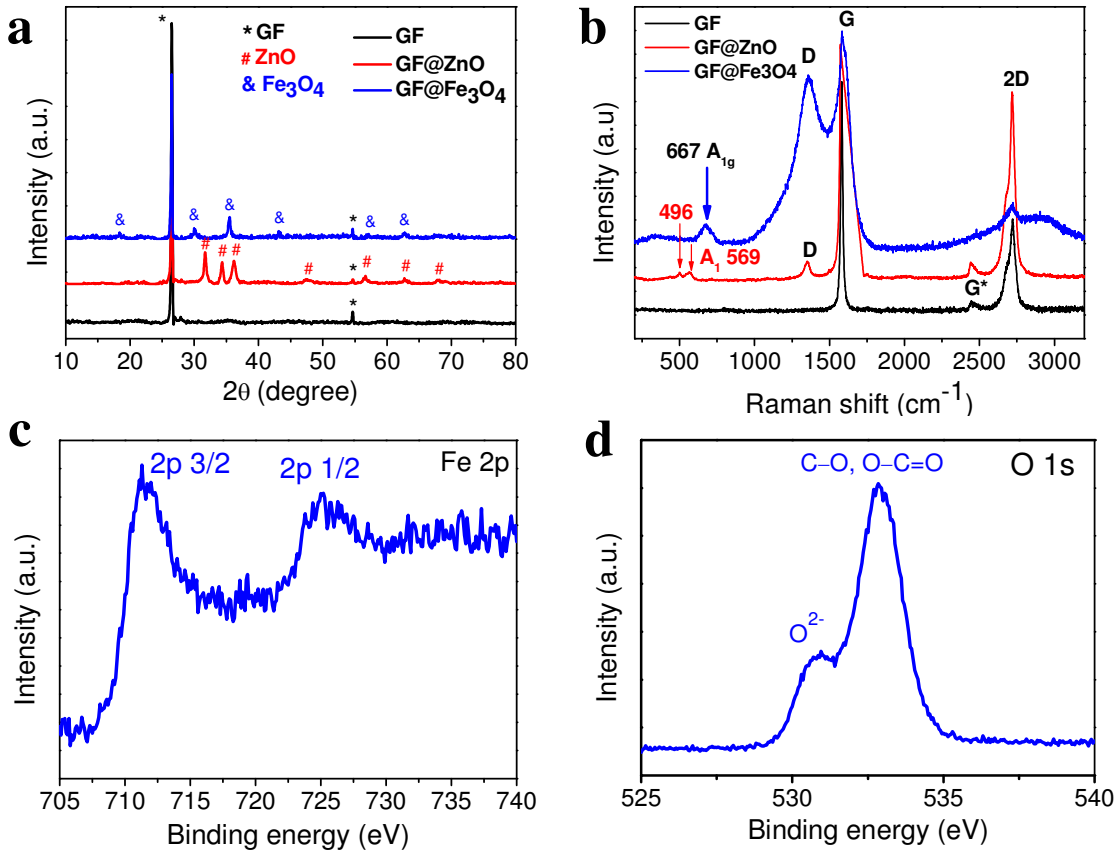

Figure 2. Sample characterization. (a) X-ray diffraction patterns of the graphene form (GF), graphene foam supported ZnO (GF@ZnO) and graphene foam supported Fe_3O_4 (GF@Fe_3O_4) nanostructures. (b) Raman spectra of the GF, GF@ZnO and GF@Fe_3O_4 nanostructures. X-ray photoelectron spectroscopy of (c) the Fe 2p states and (d) of the O 1s state in Fe_3O_4.

electron transfer. More diffraction peaks show up after ZnO coating by ALD, corresponding to the hexagonal structure of ZnO (JCPDS card 36-1451). The ALD ZnO is crystalline due to the high deposition temperature. After the replacement of ZnO into Fe_3O_4, the diffraction peaks of ZnO disappear, while only the peaks of Fe_3O_4 corresponding to the magnetite structure can be

seen (JCPDS, card 19-0629). Raman spectra in Fig. 2b show three typical peaks of graphene, centered at 1580, 2550, and 2720 cm^{-1} and corresponding to the G, G* and 2D band, respectively.[37, 38,39] The lack of the trace of the disorder-induced D band at 1350 cm^{-1} indicates the high quality of the graphene foam. Also the Raman intensity of the G band is much higher than the 2D band, which is consistent with the multilayer property of graphene foam.[27, 36, 40] This makes it rigid to serve as the scaffold for battery electrodes. After the ZnO deposition, two additional major peaks appear at 496 and 569 cm^{-1}. The later corresponds to ZnO A_1(LO) phonon,[41] and the former might be due to the interaction between ZnO and graphene foam. It is noted that, after the ZnO deposition, the graphene D band shows up, which might be due to the introduction of defects during ozone plasma treatment and ZnO deposition. In the spectrum of the final GF@Fe_3O_4 sample, the Raman modes of Fe_3O_4 can be clearly identified at 667 cm^{-1}, corresponding to the A_{1g} mode.[9] The D band of graphene foam becomes more intensive due to the introduction of more defects, while the higher-order 2D band is greatly broadened although the intensity is reduced, which might also originate from the outmost amorphous carbon layer.[42] XPS results (Figs. 2c and d) show typical characteristics of Fe_3O_4 of the final electrode, with two peaks located at 710.9 and 724.2 eV, corresponding to the Fe $2p_{3/2}$ and $2p_{1/2}$ states, respectively.[43] The absence of the satellite peaks also corroborates the assignment of the final product to Fe_3O_4 rather than Fe_2O_3.[43] This is an important character to distinguish between Fe_3O_4 (magnetite) and γ-Fe_2O_3 (maghemite) since the two have the same crystalline structure but differ only in the valence state of iron ions. For the O 1s spectrum, the low binding energy peak centered at 530.9 eV corresponds to the O^{2-} bonded with iron, and the high energy peak at 532.2 eV can be assigned to C–O and O–C=O bonds.[44-46] A small shoulder between the two dominating peaks, around 531.2 eV, could originate from surface –OH groups. The wide scan XPS is presented in Supporting Information, Figure S1.

The detailed morphology of the GF@Fe_3O_4 bi-continuous structure is characterized using electron micrographs. As revealed by the scanning electron microscopy (SEM) images, the CVD grown graphene foam well inherits the structure of the pristine Ni foam, with 3D and porous characteristics (Figs. 3a and d). Furthermore, the graphene foams are very light and flexible. The thickness or the mass of the graphene foam (from 0.1 mg/cm to 0.8 mg/cm) can be tuned by adjusting the growth time. After ZnO coating, the morphology of graphene foam shows no obvious change, indicating that the coating is conformal and homogeneous (Fig 3b). The tiny

particle type compact ZnO layer on graphene foam can be revealed by the high magnification SEM and TEM images, as illustrated in Fig. 3c and Fig. 4b. The excellent coating the ZnO will result in a good coverage of Fe_3O_4 on graphene foam. More importantly, the loading of the Fe_3O_4 can be tuned by varying the ZnO deposition cycles. Figure S2 shows the SEM and TEM images of the graphene foam supported FeOOH by using ZnO layer of 10, 30 and 50 nm thickness with bath in $FeCl_3$ solution for 24h without glucose, ZnO is transformed into FeOOH due to hydrolysis of $FeCl_3$. After this and final transformation into Fe_3O_4, the graphene foam surface becomes rough, which can be seen under even low magnification SEM image in Fig. 3c, covered by small particles, as revealed by high magnification SEM (Fig. 3f) and TEM (Figs. 4c and d and S3) images. Each individual particle is around 30 nm in diameter and is single crystalline, as shown by the HRTEM image in Fig. 4e and selected area electron diffraction pattern in Fig. 4f. The distance of the lattice fringes is around 0.25 nm, corresponding to the (311) plane of Fe_3O_4. By a closer inspection of the Fe_3O_4 nanocrystallites, it is found that the crystallites are interconnected with each other, forming bicontinuous mesoporous nanostructure. The electron diffraction pattern from selected areas shows the characteristics of both graphene and Fe_3O_4.

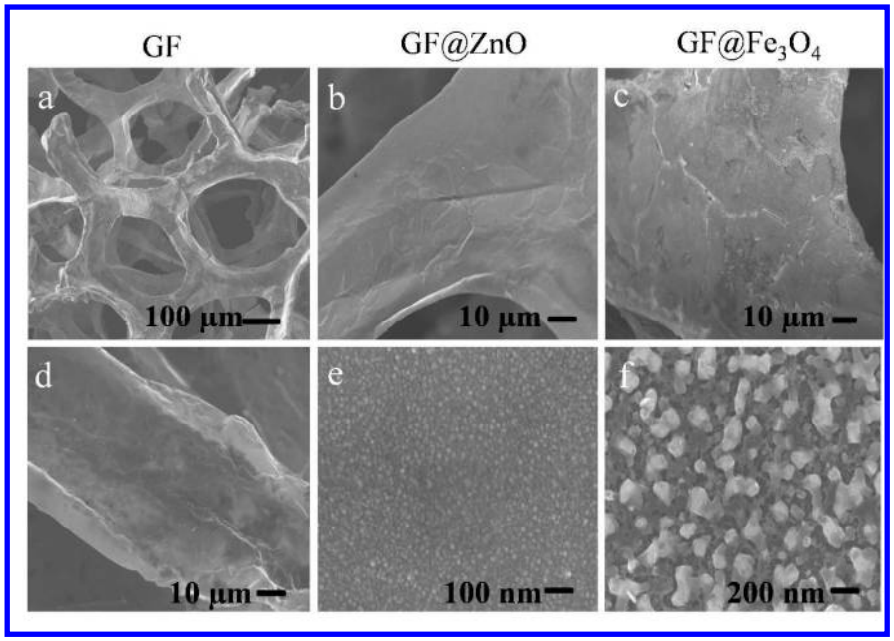

Figure 3. SEM morphology of the sample. (a, d) GF. (b, e) GF@ZnO. (c, f) GF@Fe_3O_4.

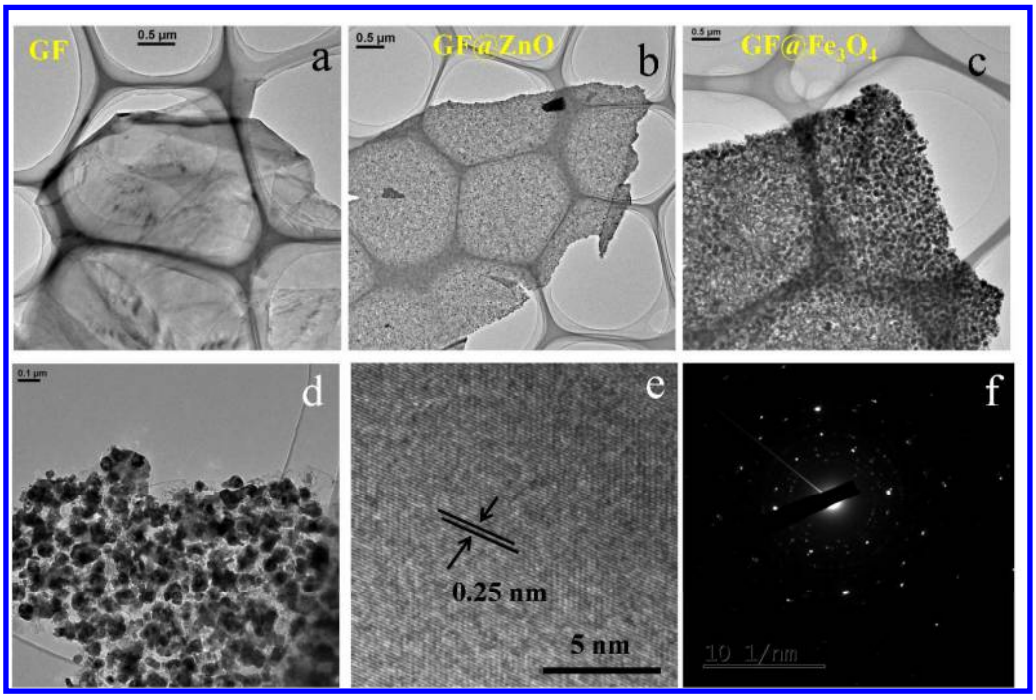

Figure 4. TEM investigation. (a) GF. (b) GF@ZnO. (c and d) GF@Fe_3O_4. (e) HRTEM of an individual Fe_3O_4 nanoparticle. (f) SAED patterns of GF@Fe_3O_4.

Lithium storage performance. The electrochemical property of the GF@Fe_3O_4 electrodes was systematically investigated by assembling them into coin cells with the lithium foil as the reference electrode. The charge storage behavior was first characterized by cyclic voltammetry (CV). As shown in Fig 5a, in the first discharge process two well defined reduction peaks can be resolved at 0.67 V and 0.27 V, respectively, corresponding to the structure transition induced by lithium intercalation ($Fe_3O_4 + xLi^+ + xe^- \rightarrow Li_xFe_3O_4$) and the further reduction of $Li_xFe_3O_4$ to Fe(0) by conversion reaction [$Li_xFe_3O_4 + (8\text{-}x)\ Li^+ + (8\text{-}x)\ e^- \rightarrow 4Li_2O + 3Fe$], which have been well elaborated in previous studies.[7, 47, 48] In the subsequent cycles, redox reactions of lithium insertion/extraction are highly reversible, where the cathodic lithium insertion mainly occurs at 1.1 and 0.75 V, and the anodic lithium extraction occurs at 1.6 and 2.3 V due to the electrochemical reduction/oxidation ($Fe_3O_4 \leftrightarrow Fe$) reactions accompanying with lithium ion insertion (lithiation) and extraction (delithiation).[47, 48] Apart from the reaction peaks for Fe_3O_4, the CV profiles also show another pair of redox peaks located at 0.1 and 0.27 V, which correspond to the lithiation and dilithiation of graphene foam, respectively.[26, 49] It is noted that

this new plateau position differs from the previous graphene samples prepared by wet chemical methods.[50, 51] The intensity of the GF peaks is very low compared to those for Fe_3O_4. This is because of the high loading of Fe_3O_4, as also confirmed by the TGA measurement that the Fe_3O_4 takes 80% of the total mass of the composite (Fig. S4). It is noteworthy that the second and third cycle of the voltage-current curves almost overlaps with each other, indicating the stable performance of the electrode in subsequent cycles. The discharge-charge voltage-capacity profiles (Fig. 5b) show two voltage plateaus at 0.4 V and 0.65 V in the first cycle, which correspond to irreversible reactions and are not observed in the 2nd cycle, in agreement with the CV results. The composite electrode shows a high initial capacity of 1192 mAh/g and a lower capacity of 785 mAh/g in the second cycle, resulting in a 1st-cycle columbic efficiency of around 66%. The capacity loss is most likely due to the irreversible reactions by the formation of the solid electrolyte interface (SEI) layer,[11, 13, 25] as seen also from the shape difference between the discharge voltage profiles of the first and second cycle. It is also observed that, the low-potential plateau turns to broad upon a deep cycling (300–500th) whereas the high-potential one almost disappears, as observed similarly also in the previous reports.[48, 52] This phenomenon might be indicative of a change in the lithium ion insertion and extraction reactions after deep cycles. Further in-depth investigation is needed.

In order to evaluate the cycle stability of the electrodes, the discharge–charge measurements were carried out at 1C rate up to 500 cycles in ambient condition. Figure 5c shows the extremely high cyclic stability of the hybrid electrode. For comparison, controlled cells with pure graphene foam electrode were also tested. The capacity of the composite electrode shows a trivial decrease during the first 100 cycles followed by slow increase in the subsequent steps. A capacity of 870 mAh/g is retained till 500 cycles at 1C discharge and charge rate. This is remarkable compared to the previous reports in cycling stability.[9, 10, 48] Overall the electrode shows relatively stable performance, and the capacity is around trice that of the pure graphene foam electrode, as a result of dominating contribution by Fe_3O_4 (Fig 5c). As for the pure Fe_3O_4 electrode, the cycle life in literature is less than 100 cycles even at 0.5C capacity rate.

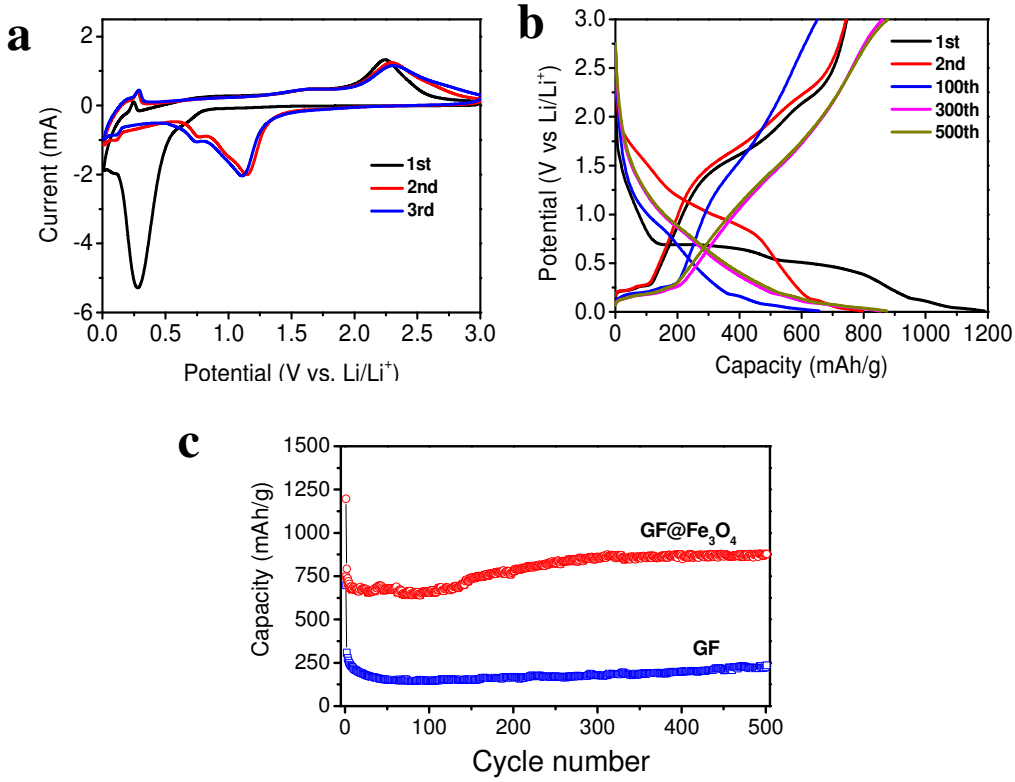

Figure 5. Electrochemical properties of the GF@Fe_3O_4 LIB electrodes. (a) cyclic voltammetry (CV) curves of the GF@Fe_3O_4 electrode. (b) discharge-charge voltage-capacity profiles of the GF@Fe_3O_4 electrode at 1C rate. (c) Cycling profiles of the GF and GF@Fe_3O_4 electrodes at 1C rate.

To test the ultrafast charging and discharging capability of the electrodes, the galvanostatic discharge (lithium insertion) – charge (lithium extraction) measurements were carried out at various C rates. Figures 6a and b show the decrease in the capacity with increasing C rates. A high capacity of 800 mAh/g can be measured when the C rate reduces back from 60C to 1C, indicating a high stability as well as excellent reversibility. Noticeably, the electrode delivers a capacity of 190 mAh/g at 60 C, implying the potential of full charge in about 1 min. This has not been reported ever for Fe_3O_4 based electrodes for LIB. The cyclic capacity profile at both 6C and 10C rates till 500 cycles are reasonably good, remaining at ~400 and 300 mAh/g, respectively (Fig. 6c), which is much better than conventional graphite anodes at such high C rates.

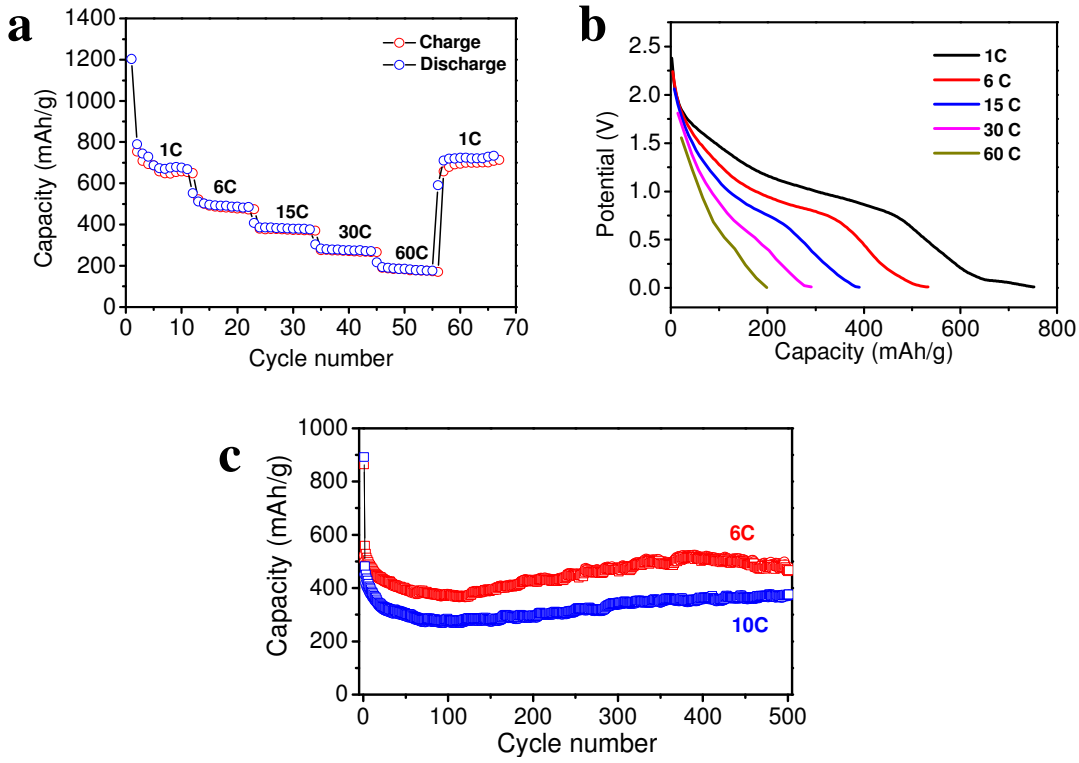

Figure 6. Rate capability of the GF@Fe_3O_4 LIB electrode. (a) Capacity of the GF@Fe_3O_4 electrode at different discharge and charge rates. (b) Discharge-charge voltage-capacity profiles of the GF@Fe_3O_4 electrode at current rates. (c) Cycling profiles of the GF@Fe_3O_4 electrodes at 6 and 10C rates.

To understand the possible synergistic effect in the composite electrode, the sample was characterized after 500 cycles discharge and charge at 1C. The electrochemical impedance spectroscopy result (Fig. S5a) shows that the impedance of the electrode decreases evidently after cycling. This has been commonly observed for metal oxide LIB electrodes, and herein could be due to the reduction of Fe_3O_4 into Fe by the irreversible reactions. Despite somewhat pulverization of the electrodes due to repeated lithiation-dilithiation, the bicontinuous mesoporous Fe_3O_4 layer still adheres firmly to the surface of graphene foam, and the individual Fe_3O_4 nanocrystallites can still be well recognized (Fig. S5b and c).

It is noted that the capacity increases gradually during cycling. This phenomenon has also been observed previously for metal oxide electrodes in long time cycles,[10, 53-56] but there is so far

no consensus on the reason. We propose three possibilities as follows. (*i*) The pulverization will increase the surface area of the electrode and release more active sites for lithium storage. So the capacity increases, given that the pulverized particles are still attached to the graphene foam. (*ii*) The decrement of capacity in the initial stage is accompanied with irreversible reactions that generate Fe nanoparticles.[56] The metallic particles will increase the overall conductivity of the electrodes (in accordance with the impedance result, Figure S5a). As a result, the charge transfer kinetics will also be improved, resulting in the increment of the capacity in the following cycles. (*iii*) The decomposition of the electrolyte forms an organic polymeric/gel-like SEI layer on the electrode surface.[10, 53, 54] This SEI layer could improve the mechanical cohesion of the active materials without hindering the ion transfer. The SEI layer could also provide excess lithium ion storage sites by a so called "pseudo-capacitance-type" behaviour, especially in the low potential region.

Interestingly, the addition of glucose in the $FeCl_3$ solution has an effect to the crystal phase and morphology of the iron oxide particles. When the glucose solution was not added, the resulting material is rice-shaped Fe_2O_3 nanoparticles. The cyclic properties of both types of GF-supported electrodes are shown in Figure S6. Clearly, the GF@Fe_2O_3 electrode has a much lower and less stable capacity during cycles up to 500 times.

The outstanding performance of the GF@Fe_3O_4 electrodes can be attributed to the rational design of the mesoscale structure that takes advantages in both electrical conductivity and structural stability (see discussion in the introduction part). We would like to restate that, this ALD ZnO-assisted method for Fe_3O_4 bi-continuous nanocrystallite films can be generalized to other carbon substrates or even metal oxide nanowires. The most determinant step is the ZnO, which affects the homogeneity of the resulting iron oxide layers and substantially increase the loading of coated active materials. To prove this, we have repeated the experiments on chemically produced graphene oxide and carbon nanotubes. As illustrated in Fig. S7, the coatings of Fe_3O_4 are also homogenous. Note that the total mass of the electrodes here is still very low, which also hinds the real application of the electrodes. However, this might be overcome by stacking such GF-supported active material electrodes to form a multilayer film, so as to increase the energy density.

In conclusion, we have demonstrated a new strategy to achieve bicontinous mesoporous Fe_3O_4 nanostructures on 3D graphene foams for the LIB application. Due to the rational design and the unique mesoscale structure, the electrodes show a high capacity of 785 mAh g^{-1} at 1C discharge-charge rate and could maintain this high capacity up to 500 cycles. This fabrication method is compatible with many other carbon substrates, such as graphene oxides and carbon nanotubes. The homogeneous grafting of iron oxides with tunable loadings onto carbon supports is exclusively attributed to the uniform coating of ZnO by ALD.

Methods

Growth of 3D graphene foams. The growth of the 3D graphene foams was achieved by chemical vapour deposition (CVD) using First Nano's EasyTube 3000 System with a modified recipe from previous methods.[27, 40] Briefly, the 8 × 8 cm size nickel foams were directly used as the scaffold templates and were loaded into a 5 inch quartz tube inside a horizontal tube furnace. Then the furnace was heated to 1,000 ºC under an Ar (500 sccm) plus H_2 (200 sccm) atmosphere and stayed at the peak temperature for 5 min in order to clean the nickel foam surfaces and eliminate the thin surface oxide layer. After the annealing procedure, a small amount of CH_4 was introduced into the reaction tube at ambient pressure. The flow rates of CH_4, H_2 and Ar were 50, 100 and 800 s.c.c.m, respectively. After 2 min growth, the samples were rapidly cooled to room temperature at a rate of ~100 $^{\circ}C$ min^{-1} under a constant flow of Ar (500 sccm) and H_2 (200 sccm). Free-standing GF foam was obtained via acidic etching of nickel backbone in $Fe(NO_3)_3$/HCl mixture solution.

Atomic layer deposition of ZnO and formation of Fe_3O_4 nanostructure. Before ALD deposition, the graphene foams were treated with oxygen plasma. The reactive ion etching (RIE) was performed on a March PX-250 plasma etching system at 100 sccm oxygen gas flow, 70 mTorr, and 100 W power density for 5 min. The plasma processed graphene foams were then directly transferred to the ALD chamber for ZnO deposition. The ZnO deposition was done by Beneq TFS 200 system at 200 °C using diethyl zinc (DEZ, 99.99%, Sigma Aldrich) and H_2O as the Zn and O precursors, respectively. The thickness was controlled by the cycles; in this work 60, 180, and 300 cycles were used to obtain around 10, 30, and 50 nm thickness, respectively.

The ALD ZnO coated graphene foams were immersed into a mixture of $FeCl_3$ (30 mM) and glucose solution (30 mM) for 24 h to convert ZnO completely into FeOOH. Then the samples were annealed in an

Ar atmosphere at 400 °C for 2 h in order to transform FeOOH to Fe_3O_4 and, simultaneously, glucose to amorphous carbon.

Structure and morphology characterization. The morphology of the samples was characterized using a JEOL JSM 6700F field emission scanning electron microscopy (SEM) and a JEOL JEM-2010 transmission electron microscopy (TEM). The XPS measurements were performed with a VG ESCALAB 220i-XL system using a monochromatic Al Ka1 source (1486.6 eV). All XPS spectra were obtained in the constant pass energy (CPA) mode. The pass energy of analyzer was set to be 10 eV to have high measurement accuracy. The binding energy scale was calibrated with pure Au, Ag and Cu by setting the Au $4f_{7/2}$, Ag $3d_{5/2}$ and Cu $2p_{3/2}$ at binding energy of 84.0, 368.3, and 932.7 eV, respectively. Thermogravimetric analysis (TGA) was conducted on a TGA Q500 (Thermal Analysis Instruments, Burlington, MA) machine in O_2, with a flow rate of 60 ml min^{-1} and a temperature ramp rate of 10 ºC min^{-1} from room temperature to 800 ºC.

Electrochemical performance test. Standard CR2032-type coin cells were assembled in an Ar-filled glovebox (Mbraun, Unilab, Germany) by directly using the as-fabricated graphene foam supported Fe_3O_4 nanostructures (GF@Fe3O4) as the electrodes, without using any binder or additives. The lithium metal circular foil (0.59 mm thick) was used as the counter electrode and a microporous polypropylene membrane served as the separator. The electrolyte consisted of 1 M $LiPF_6$ in ethylene carbonate (EC) and diethyl carbonate (DEC) (1:1 by volume). Before the electrochemical measurements, the assembled cells were aged in the glove box for 10 h. Galvanostatical discharge-charge experiments were performed at different current densities in the voltage range of 0.01 – 3.00 V with a multichannel battery tester (Neware, China). The cyclic voltammetry (CV) and electrochemical impedance spectroscopy (EIS) were measured using an electrochemical workstation (CHI760D, Chenhua, Shanghai).

ASSOCIATED CONTENT

Supporting Information Available: Wide scan XPS of the GF@Fe_3O_4 sample, SEM and TEM images of the samples obtained with three different ZnO layer thicknesses, thermogravimetric analysis (TGA) of GF@Fe_3O_4 electrode, EIS and SEM images of the GF@Fe_3O_4 electrode after 500 cycles, comparison of capacities between GF@Fe_3O_4 and GF@Fe_2O_3 electrodes up to 500 cycles, SEM and TEM images of iron oxide nanoparticles obtained on other types of substrates (graphene oxide flakes and carbon nanotubes). This material is available free of charge *via* the Internet at http://pubs.acs.org.

AUTHOR INFORMATION

J.S. Luo and J. L. Liu contribute equally to this work.

Corresponding Authors.

* Email: fanhj@ntu.edu.sg (H.J. F)

Notes

The authors declare no competing financial interest.

ACKNOWLEDGEMENTS

H. J. Fan thanks the financial support by SERC Public Sector Research Funding (Grant number 1121202012), Agency for Science, Technology, and Research (A*STAR). H. J. Fan and Z. X. Shen appreciate the support by Singapore Ministry of Education Academic Research Fund Tier 3 (MOE2011-T3-1-005). H. Zhang acknowledges the support by Singapore MOE under AcRF Tier 2 (ARC 26/13, No. MOE2013-T2-1-034), AcRF Tier 1 (RG 61/12), and NTU Start-Up Grant (M4080865). This research is also funded by the Singapore National Research Foundation and the publication is supported under the Campus for Research Excellence And Technological Enterprise (CREATE) programme (Nanomaterials for Energy and Water Management). The authors also acknowledge partial financial support from the Energy Research Institute @NTU and the help from Ting Yu and his group members with the usage of glove box and oxygen plasma etcher.

References

1. Armand, M.; Tarascon, J. M., Building better batteries. *Nature* **2008,** *451* (7179), 652-657.

2. Kang, B.; Ceder, G., Battery materials for ultrafast charging and discharging. *Nature* **2009,** *458* (7235), 190-193.

3. Poizot, P.; Laruelle, S.; Grugeon, S.; Dupont, L.; Tarascon, J. M., Nano-sized transition-metal oxides as negative-electrode materials for lithium-ion batteries. *Nature* **2000,** *407* (6803), 496-499.

4. Taberna, P. L.; Mitra, S.; Poizot, P.; Simon, P.; Tarascon, J. M., High rate capabilities Fe3O4-based Cu nano-architectured electrodes for lithium-ion battery applications. *Nat Mater* **2006,** *5* (7), 567-573.

5. Kim, I. T.; Magasinski, A.; Jacob, K.; Yushin, G.; Tannenbaum, R., Synthesis and Electrochemical Performance of Reduced Graphene Oxide/Maghemite Composite Anode for Lithium Ion Batteries. *Carbon* **2013,** *52* (0), 56-64.

6. Chen, J.; Xu, L.; Li, W.; Gou, X., α-Fe2O3 Nanotubes in Gas Sensor and Lithium-Ion Battery Applications. *Adv. Mater.* **2005,** *17* (5), 582-586.

7. Reddy, M. V.; Yu, T.; Sow, C. H.; Shen, Z. X.; Lim, C. T.; Subba Rao, G. V.; Chowdari, B. V. R., α-Fe2O3 Nanoflakes as an Anode Material for Li-Ion Batteries. *Adv. Funct. Mater.* **2007,** *17* (15), 2792-2799.

8. Larcher, D.; Masquelier, C.; Bonnin, D.; Chabre, Y.; Masson, V.; Leriche, J.-B.; Tarascon, J.-M., Effect of Particle Size on Lithium Intercalation into α - Fe2 O 3. *J. Electrochem. Soc.* **2003,** *150* (1), A133-A139.

9. Zhou, G.; Wang, D.-W.; Li, F.; Zhang, L.; Li, N.; Wu, Z.-S.; Wen, L.; Lu, G. Q.; Cheng, H.-M., Graphene-Wrapped Fe3O4 Anode Material with Improved Reversible Capacity and Cyclic Stability for Lithium Ion Batteries. *Chem. Mater.* **2010,** *22* (18), 5306-5313.

10. Wu, Y.; Wei, Y.; Wang, J.; Jiang, K.; Fan, S., Conformal Fe3O4 Sheath on Aligned Carbon Nanotube Scaffolds as High-Performance Anodes for Lithium Ion Batteries. *Nano Lett.* **2013,** *13* (2), 818-823.

11. Kang, E.; Jung, Y. S.; Cavanagh, A. S.; Kim, G.-H.; George, S. M.; Dillon, A. C.; Kim, J. K.; Lee, J., Fe3O4 Nanoparticles Confined in Mesocellular Carbon Foam for High Performance Anode Materials for Lithium-Ion Batteries. *Adv. Funct. Mater.* **2011,** *21* (13), 2430-2438.

12. Ban, C.; Wu, Z.; Gillaspie, D. T.; Chen, L.; Yan, Y.; Blackburn, J. L.; Dillon, A. C., Nanostructured Fe3O4/SWNT Electrode: Binder-Free and High-Rate Li-Ion Anode. *Adv. Mater.* **2010,** *22* (20), E145-E149.

13. Chan, C. K.; Peng, H.; Liu, G.; McIlwrath, K.; Zhang, X. F.; Huggins, R. A.; Cui, Y., High-performance lithium battery anodes using silicon nanowires. *Nat Nano* **2008,** *3* (1), 31-35.

14. Luo, Y.; Luo, J.; Jiang, J.; Zhou, W.; Yang, H.; Qi, X.; Zhang, H.; Fan, H. J.; Yu, D. Y. W.; Li, C. M.; Yu, T., Seed-assisted Synthesis of Highly Ordered TiO2@a-Fe2O3 Core/Shell Arrays on Carbon Textiles for Lithium-Ion Battery Applications. *Energy Environ. Sci.* **2012,** *5* (4), 6559-6566.

15. Luo, J.; Xia, X.; Luo, Y.; Guan, C.; Liu, J.; Qi, X.; Ng, C. F.; Yu, T.; Zhang, H.; Fan, H. J., Rationally Designed Hierarchical TiO2@Fe2O3 Hollow Nanostructures for Improved Lithium Ion Storage. *Adv. Energy Mater.* **2013,** *3* (6), 737-743.

16. Arico, A. S.; Bruce, P.; Scrosati, B.; Tarascon, J.-M.; van Schalkwijk, W., Nanostructured materials for advanced energy conversion and storage devices. *Nat Mater* **2005,** *4* (5), 366-377.

17. Magasinski, A.; Dixon, P.; Hertzberg, B.; Kvit, A.; Ayala, J.; Yushin, G., High-performance lithium-ion anodes using a hierarchical bottom-up approach. *Nat Mater* **2010,** *9* (4), 353-358.

18. Zhang, H.; Yu, X.; Braun, P. V., Three-dimensional bicontinuous ultrafast-charge and -discharge bulk battery electrodes. *Nat Nano* **2011,** *6* (5), 277-281.

19. Koo, B.; Xiong, H.; Slater, M. D.; Prakapenka, V. B.; Balasubramanian, M.; Podsiadlo, P.; Johnson, C. S.; Rajh, T.; Shevchenko, E. V., Hollow Iron Oxide Nanoparticles for Application in Lithium Ion Batteries. *Nano Lett.* **2012,** *12* (5), 2429-2435.

20. Song, Y.; Qin, S.; Zhang, Y.; Gao, W.; Liu, J., Large-Scale Porous Hematite Nanorod Arrays: Direct Growth on Titanium Foil and Reversible Lithium Storage. *J. Phys. Chem. C* **2010,** *114* (49), 21158-21164.

21. Lei, D.; Zhang, M.; Qu, B.; Chen, L.; Wang, Y.; Zhang, E.; Xu, Z.; Li, Q.; Wang, T., [small alpha]-Fe2O3 nanowall arrays: hydrothermal preparation, growth mechanism and excellent rate performances for lithium ion batteries. *Nanoscale* **2012,** *4* (11), 3422-3426.

22. Yang, S.; Sun, Y.; Chen, L.; Hernandez, Y.; Feng, X.; Müllen, K., Porous Iron Oxide Ribbons Grown on Graphene for High-Performance Lithium Storage. *Sci. Rep.* **2012,** *2*, 427.

23. Wang, B.; Chen, J. S.; Wu, H. B.; Wang, Z.; Lou, X. W., Quasiemulsion-Templated Formation of α-Fe2O3 Hollow Spheres with Enhanced Lithium Storage Properties. *J. Am. Chem. Soc.* **2011,** *133* (43), 17146-17148.

24. Liu, J.; Zhou, W.; Lai, L.; Yang, H.; Hua Lim, S.; Zhen, Y.; Yu, T.; Shen, Z.; Lin, J., Three Dimensionals α-Fe2O3/Polypyrrole (Ppy) Nanoarray as Anode for Micro Lithium Ion Batteries. *Nano Energy* **2013,** *2* (5), 726-732.

25. Zhu, X.; Zhu, Y.; Murali, S.; Stoller, M. D.; Ruoff, R. S., Nanostructured Reduced Graphene Oxide/Fe2O3 Composite As a High-Performance Anode Material for Lithium Ion Batteries. *ACS Nano* **2011,** *5* (4), 3333-3338.

26. Li, N.; Chen, Z.; Ren, W.; Li, F.; Cheng, H.-M., Flexible graphene-based lithium ion batteries with ultrafast charge and discharge rates. *Proc. Natl. Acad. Sci.* **2012,** *109* (43), 17360-17365.

27. Chen, Z.; Ren, W.; Gao, L.; Liu, B.; Pei, S.; Cheng, H.-M., Three-dimensional flexible and conductive interconnected graphene networks grown by chemical vapour deposition. *Nat Mater* **2011,** *10* (6), 424-428.

28. Liu, J.; Li, Y.; Fan, H.; Zhu, Z.; Jiang, J.; Ding, R.; Hu, Y.; Huang, X., Iron Oxide-Based Nanotube Arrays Derived from Sacrificial Template-Accelerated Hydrolysis: Large-Area Design and Reversible Lithium Storage. *Chem. Mater.* **2009,** *22* (1), 212-217.

29. Karuturi, S. K.; Luo, J.; Cheng, C.; Liu, L.; Su, L. T.; Tok, A. I. Y.; Fan, H. J., A Novel Photoanode with Three-Dimensionally, Hierarchically Ordered Nanobushes for Highly Efficient Photoelectrochemical Cells. *Adv. Mater.* **2012,** *24* (30), 4157-4162.

30. Marichy, C.; Bechelany, M.; Pinna, N., Atomic Layer Deposition of Nanostructured Materials for Energy and Environmental Applications. *Adv. Mater.* **2012,** *24* (8), 1017-1032.

31. Luo, J.; Karuturi, S. K.; Liu, L.; Su, L. T.; Tok, A. I. Y.; Fan, H. J., Homogeneous Photosensitization of Complex TiO2 Nanostructures for Efficient Solar Energy Conversion. *Sci. Rep.* **2012,** *2*, 451.

32. Wang, X.; Tabakman, S. M.; Dai, H., Atomic Layer Deposition of Metal Oxides on Pristine and Functionalized Graphene. *J. Am. Chem. Soc.* **2008,** *130* (26), 8152-8153.

33. Jandhyala, S.; Mordi, G.; Lee, B.; Lee, G.; Floresca, C.; Cha, P.-R.; Ahn, J.; Wallace, R. M.; Chabal, Y. J.; Kim, M. J.; Colombo, L.; Cho, K.; Kim, J., Atomic Layer Deposition of Dielectrics on Graphene Using Reversibly Physisorbed Ozone. *ACS Nano* **2012,** *6* (3), 2722-2730.

34. Martinson, A. B. F.; DeVries, M. J.; Libera, J. A.; Christensen, S. T.; Hupp, J. T.; Pellin, M. J.; Elam, J. W., Atomic Layer Deposition of Fe2O3 Using Ferrocene and Ozone. *J. Phys. Chem. C* **2011,** *115* (10), 4333-4339.

35. Li, X.; Fan, N. C.; Fan, H. J., A Micro-pulse Process of Atomic Layer Deposition of Iron Oxide Using Ferrocene and Ozone Precursors and Ti-Doping. *Chem. Vap. Deposition* **2013,** *19* (4-6), 104-110.

36. Dong, X.-C.; Xu, H.; Wang, X.-W.; Huang, Y.-X.; Chan-Park, M. B.; Zhang, H.; Wang, L.-H.; Huang, W.; Chen, P., 3D Graphene–Cobalt Oxide Electrode for High-Performance Supercapacitor and Enzymeless Glucose Detection. *ACS Nano* **2012,** *6* (4), 3206-3213.

37. Mafra, D. L.; Samsonidze, G.; Malard, L. M.; Elias, D. C.; Brant, J. C.; Plentz, F.; Alves, E. S.; Pimenta, M. A., Determination of LA and TO phonon dispersion relations of graphene near the Dirac point by double resonance Raman scattering. *Phys. Rev. B* **2007,** *76* (23), 233407.

38. Malard, L. M.; Pimenta, M. A.; Dresselhaus, G.; Dresselhaus, M. S., Raman spectroscopy in graphene. *Phys. Rep.* **2009,** *473* (5–6), 51-87.

39. The G peak is associated with the doubly degenerate (iTO and LO) phonon mode (with E2g symmetry) at the Brillouin zone center. The disorder-induced D band involves one iTO phonon and one defect. Both the G' (also called 2D band) and G* bands come from a double resonance Raman scattering process. The G′ involves two iTO phonons near the K point, while the G* band involves one iTO and one LA phonon. (37,38)

40. Cao, X.; Shi, Y.; Shi, W.; Lu, G.; Huang, X.; Yan, Q.; Zhang, Q.; Zhang, H., Preparation of Novel 3D Graphene Networks for Supercapacitor Applications. *Small* **2011,** *7* (22), 3163-3168.

41. Calleja, J. M.; Cardona, M., Resonant Raman scattering in ZnO. *Phys. Rev. B* **1977,** *16* (8), 3753-3761.

42. Ferrari, A. C.; Robertson, J., Interpretation of Raman spectra of disordered and amorphous carbon. *Phys. Rev. B* **2000,** *61* (20), 14095-14107.

43. Fujii, T.; de Groot, F. M. F.; Sawatzky, G. A.; Voogt, F. C.; Hibma, T.; Okada, K., In situ XPS analysis of various iron oxide films grown by NO2-assisted molecular-beam epitaxy. *Phys. Rev. B* **1999,** *59* (4), 3195-3202.

44. McCafferty, E.; Wightman, J. P., Determination of the concentration of surface hydroxyl groups on metal oxide films by a quantitative XPS method. *Surf. Interface Anal.* **1998,** *26* (8), 549-564.

45. Yamashita, T.; Hayes, P., Analysis of XPS Spectra of Fe2+ and Fe3+ Ions in Oxide Materials. *Appl. Surf. Sci.* **2008,** *254* (8), 2441-2449.

46. Bhargava, G.; Gouzman, I.; Chun, C. M.; Ramanarayanan, T. A.; Bernasek, S. L., Characterization of the "native" surface thin film on pure polycrystalline iron: A high resolution XPS and TEM study. *Appl. Surf. Sci.* **2007,** *253* (9), 4322-4329.

47. Jia, X.; Chen, Z.; Cui, X.; Peng, Y.; Wang, X.; Wang, G.; Wei, F.; Lu, Y., Building Robust Architectures of Carbon and Metal Oxide Nanocrystals toward High-Performance Anodes for Lithium-Ion Batteries. *ACS Nano* **2012,** *6* (11), 9911-9919.

48. He, C.; Wu, S.; Zhao, N.; Shi, C.; Liu, E.; Li, J., Carbon-Encapsulated Fe3O4 Nanoparticles as a High-Rate Lithium Ion Battery Anode Material. *ACS Nano* **2013,** *7* (5), 4459-4469.

49. Frackowiak, E.; Béguin, F., Electrochemical Storage of Energy in Carbon Nanotubes and Nanostructured Carbons. *Carbon* **2002,** *40* (10), 1775-1787.

50. Chen, W. F.; Li, S. R.; Chen, C. H.; Yan, L. F., Self-Assembly and Embedding of Nanoparticles by In Situ Reduced Graphene for Preparation of a 3D Graphene/Nanoparticle Aerogel. *Adv. Mater.* **2011,** *23* (47), 5679-5683.

51. Li, B.; Cao, H.; Shao, J.; Qu, M., Enhanced anode performances of the Fe3O4-Carbon-rGO three dimensional composite in lithium ion batteries. *Chem. Commun*. **2011,** *47* (37), 10374-10376.

52. Wang, P. C.; Ding, H. P.; Bark, T.; Chen, C. H., Nanosized alpha-Fe2O3 and Li-Fe composite oxide electrodes for lithium-ion batteries. *Electrochim. Acta* **2007,** *52* (24), 6650-6655.

53. Laruelle, S.; Grugeon, S.; Poizot, P.; Dollé, M.; Dupont, L.; Tarascon, J.-M., On the Origin of the Extra Electrochemical Capacity Displayed by MO/Li Cells at Low Potential. *J. Electrochem. Soc.* **2002,** *149* (5), A627-A634.

54. Wang, Z.; Luan, D.; Madhavi, S.; Hu, Y.; Lou, X. W., Assembling carbon-coated [small alpha]-Fe2O3 hollow nanohorns on the CNT backbone for superior lithium storage capability. *Energy Environ. Sci*. **2012,** *5* (1), 5252-5256.

55. Yu, Y.; Chen, C.-H.; Shui, J.-L.; Xie, S., Nickel-Foam-Supported Reticular CoO–Li2O Composite Anode Materials for Lithium Ion Batteries. *Angew. Chem. Int. Ed*. **2005,** *44* (43), 7085-7089.

56. Huang, X.; Chen, J.; Lu, Z.; Yu, H.; Yan, Q.; Hng, H. H., Carbon inverse opal entrapped with electrode active nanoparticles as high-performance anode for lithium-ion batteries. *Sci. Rep.* **2013,** *3*, 2317.